

# Formulation and Visualization of Bus Voltage-Var Safety Regions for a Power System

Qiupin Lai<sup>ID</sup>, Student Member, IEEE, Chengxi Liu<sup>ID</sup>, Senior Member, IEEE, and Kai Sun<sup>ID</sup>, Senior Member, IEEE

**Abstract**—This letter studies formulations on the safety regions of the voltage and reactive power (Volt/Var) of each bus in a power system by nonlinear network decomposition and proposes visualizations of these regions for operators to monitor the Volt/Var safety of the system. Unlike the conventional approach that searches for boundaries of such regions by a large number of repeated power flow calculations, the proposed method takes an analytical approach so as to avoid repeated calculations. Firstly, the power network is decomposed into a set of two-bus channels, where a complex-valued index is introduced to represent the Volt/Var status with each channel. Then, by using a scalable holomorphic embedding method, the trajectories of the indices of all channels are obtained, which together predict Volt/Var safety of the entire system under prospective operating conditions. Next, boundaries of the Volt/Var safety regions are derived and visualized to monitor the margin information of voltage stability and control. Finally, the effectiveness of the proposed method is validated on the IEEE 14-bus system in detail.

**Index Terms**—Reactive power boundary, safety region, voltage boundary.

## I. INTRODUCTION

WITH the development of the social economy and the augment of power energy demand, power systems trend to be operated under heavier load and closer to their stability limits. Hence, it is critical for system operators to monitor the voltage and reactive power (Volt/Var) status in real-time at each bus and be aware of any violation so as to take a remedial control action in advance. Traditionally, system operators need to perform a large number of repeated power flow calculations [1] to check the Volt/Var status at each bus versus its safety region, which may suffer from excessive computation burden for the online applications. Although [2] reduces online time-cost by deriving the analytical voltage stability boundary offline, it can only judge the overall status of voltage stability (feasible or not) without providing Volt/Var status at each bus. Besides, power flow calculations only check the current operating condition [3] and cannot directly foresee a violation without additional sensitivity analysis. To predict the voltage violation, a vulnerability assessment method [4] is developed to locate the vulnerable bus that triggers the voltage collapse of the entire system, however, the available Var of each generator is not considered, which may result in Var violations of generators.

Manuscript received September 19, 2021; revised December 15, 2021; accepted February 12, 2022. Date of publication March 7, 2022; date of current version June 20, 2022. This work was supported by the National Natural Science Foundation of China under Project 52007133. Paper no. PESL-00243-2021. (Corresponding author: Chengxi Liu.)

Qiupin Lai and Chengxi Liu are with the School of Electrical Engineering and Automation, Wuhan University, Wuhan 430072, China (e-mail: laiqipin@whu.edu.cn; liuchengxi@whu.edu.cn).

Kai Sun is with the Department of Electrical Engineering and Computer Science, University of Tennessee, Knoxville, TN 37996 USA (e-mail: kaisun@utk.edu).

Color versions of one or more figures in this article are available at <https://doi.org/10.1109/TPWRS.2022.3156444>.

Digital Object Identifier 10.1109/TPWRS.2022.3156444

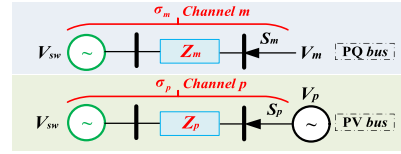


Fig. 1. Virtual two-bus channels decomposed from a multi-bus system.

To bridge the above gaps, this letter proposes analytical formulations of Volt/Var safety regions and their visualizations at each bus for both the current and prospective operating conditions. Thus, any Volt/Var violation threatening the voltage stability can be predicted visually, which is helpful for operators to formulate a remedial strategy in advance.

## II. NONLINEAR NETWORK DECOMPOSITION

The proposed method is based on nonlinear network decomposition presented in [5], which is briefly introduced below. For a multi-bus system composed of  $m$  PQ buses (sets of  $\mathcal{M}$ ),  $p$  PV buses (sets of  $\mathcal{P}$ ), and a swing bus, by constructing a virtual impedance between the swing bus and each bus, it can be decomposed into a set of virtual two-bus channels shown in Fig. 1, where each PQ or PV bus is individually on one channel connected to the swing bus via a virtual line impedance  $Z$  [5].

For channel  $i$ , a complex-valued index  $\sigma_i$  [5], which combines the parameters of virtual line impedance  $Z_i$ , swing bus voltage  $V_{sw}$  and complex power injection  $S_i$ , is introduced to represent the Volt/Var status at bus  $i$ .

$$\sigma_i = \frac{Z_i S_i^*}{|V_{sw}|^2}, \forall i \in \mathcal{M} \cup \mathcal{P} \quad (1)$$

By substituting the index  $\sigma_i$  into the power flow equation for the two-bus channel  $i$ , one can obtain (2).

$$U_i = 1 + \frac{\sigma_i}{U_i^*}, \forall i \in \mathcal{M} \cup \mathcal{P} \quad (2)$$

where  $U_i = V_i/V_{sw}$  is the normalized voltage at bus  $i$ .

Since (2) is essentially a quadratic equation, its solution is,

$$U_i = \frac{1}{2} \pm \sqrt{\frac{1}{4} + \sigma_{iR} - \sigma_{iI}^2 + j\sigma_{iI}} \\ \text{s.t. } \Delta = \frac{1}{4} + \sigma_{iR} - \sigma_{iI}^2 \geq 0 \quad (3)$$

where  $\sigma_{iR}$  and  $\sigma_{iI}$  denote the real and imaginary parts of  $\sigma_i$ , respectively.

The non-negative radicand in (3) is the necessary condition for the existence of a feasible voltage solution, which forms a parabola representing the voltage collapse on the  $\sigma$  complex plane [5], illustrated in Fig. 2.

*Remark:* First, each Volt/Var index  $\sigma_i$  for bus  $i$  is only valid for one specific operating condition. For varying operating conditions, [5] needs to resolve  $\sigma_i$  repeatedly. Second, the parabola as a boundary only tells when voltage collapse of entire system happens, the margin from

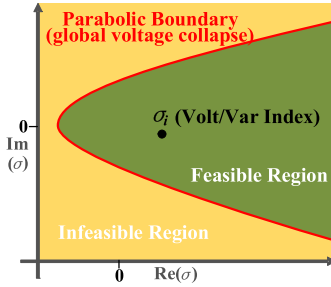


Fig. 2. Parabolic voltage collapse boundary and the Volt/Var index  $\sigma_i$ .

the index to the boundary does not indicate the Volt/Var safety at each specific bus.

To overcome the above limitations, the rest of this letter: 1) uses the trajectory of  $\sigma_i$  in Section III to trace the Volt/Var status at each bus with changing or prospective operating conditions; and 2) proposes formulation and visualization of the safety regions for the Volt/Var status at each bus in Section IV to predict a violation visually.

### III. TRAJECTORY OF VOLT/VAR INDEX

To endow the Volt/Var index  $\sigma_i$  with ability to trace the Volt/Var status with varying operating conditions, a scalable holomorphic embedding method is used to embed (2) as (4),

$$U_i(s) = 1 + \frac{\sigma_i(s)}{U_i^*(s^*)}, \forall i \in \mathcal{M} \cup \mathcal{P} \quad (4)$$

where  $s$  is a scalable factor representing the load direction, and  $\sigma_i(s) = \sigma_i[0] + \sigma_i[1]s + \dots + \sigma_i[n]s^n$  is a holomorphic function. Since (4) can return to (2) with different  $s$  values representing different operating conditions,  $\sigma_i(s)$  forms the trajectory of Volt/Var index representing the Volt/Var status at bus  $i$  under prospective operating conditions. To solve  $\sigma_i(s)$ , one can combine (4) with the holomorphic embedded power flow equations [4] and compare the coefficients of  $s$  with the same order to obtain a recursive matrix equation including the *unknown* coefficients of higher-order terms (i.e.,  $\sigma_i[n]$ ) and the *known* coefficients of lower-order terms (i.e.,  $\sigma_i[0], \sigma_i[1], \dots$ ). Then, the coefficients of  $\sigma_i(s)$  can be computed recursively (the detailed solving procedures can be found in Appendix-A). When the network topology changes, the trajectory of Volt/Var index need to be recalculated and updated, which is presented in Appendix-B. Besides, the mathematical complexity and computational effort associated with the process for recalculating  $\sigma(s)$  are analyzed in Appendix-C.

### IV. VISUALIZED BUS-SPECIFIC VOLT/VAR SAFETY REGION

In this Section, the Volt/Var safety regions are formulated and visualized on a unified complex plane together with the trajectories of Volt/Var indices, so that system operators can visually monitor the Volt/Var status of each bus and predict the violations. In general, the Volt and Var safety regions of each bus are proved to be surrounded by circles and straight lines, respectively, which is briefly illustrated in Fig. 3. The detailed derivations and analyses about the Volt/Var safety regions are presented below.

#### A. Visualization of Bus-Specific Voltage Safety Region

Firstly, assume the angle of the swing bus voltage  $V_{sw}$  is  $0^\circ$  and rearrange (4) as (5).

$$\sigma_i(s) = \left| \frac{V_i(s)}{V_{sw}} \right|^2 - \frac{V_i^*(s^*)}{V_{sw}}, \forall i \in \mathcal{M} \cup \mathcal{P} \quad (5)$$

Then, separate (5) into the real and imaginary parts,

$$\sigma_{iR}(s) = \left| \frac{V_i(s)}{V_{sw}} \right|^2 - \frac{V_{iR}(s)}{V_{sw}}; \sigma_{iI}(s) = \frac{V_{iI}(s)}{V_{sw}}, \forall i \in \mathcal{M} \cup \mathcal{P} \quad (6)$$

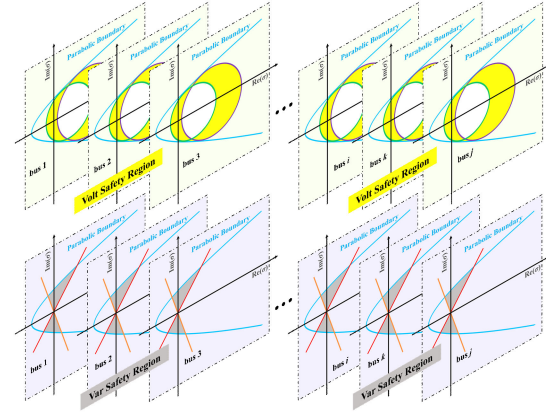


Fig. 3. Visualization of Volt/Var safety regions for each bus.

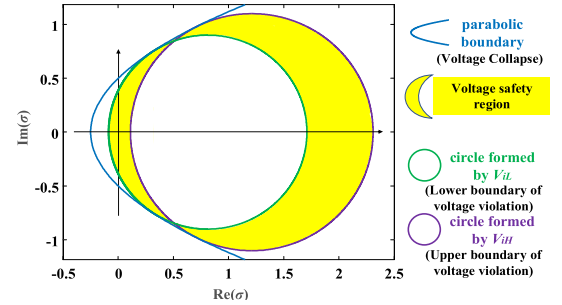


Fig. 4. Visualization of voltage safety region and boundaries.

Clearly, (6) forms a circle (7) centered at  $(|V_i(s)/V_{sw}|^2, 0)$  with radius  $|V_i(s)/V_{sw}|$ . The circle is tangent to the parabola (3), which can be proved by substituting (7) into (3).

$$\left| \frac{V_i(s)}{V_{sw}} \right|^2 = \left[ \sigma_{iR}(s) - \left| \frac{V_i(s)}{V_{sw}} \right|^2 \right]^2 + [\sigma_{iI}(s)]^2, \forall i \in \mathcal{M} \cup \mathcal{P} \quad (7)$$

According to (7), operators can preset different voltage ranges for different buses flexibly, e.g., the voltage of bus  $i$  fluctuates between  $V_{iL}$  and  $V_{iH}$ . Firstly, substitute  $V_{iL}$  and  $V_{iH}$  into (7) and visualize the results on the  $\sigma$  complex plane, one can obtain Fig. 4, where the **blue** parabola is the voltage collapse boundary, the **green** and **purple** circles denote the voltage boundaries formed by  $V_{iL}$  and  $V_{iH}$ , respectively. Then, the **yellow** part, which is surrounded by the above three boundaries, represents the voltage safety region. Thus, by plotting the trajectory of index  $\sigma_i(s)$  on Fig. 4, operators can visually monitor the voltage status and predict the voltage violations (illustrated in Section V-A).

*Remark:* By using (7), the bus voltage  $V_i(s)$  can be projected onto the  $\sigma$  complex plane as the circles formed by the voltage index  $\sigma_i(s)$ . One voltage value corresponds to one circle, for example, we assume a circle on the  $\sigma$  complex plane corresponds to  $V_i(s) = X$ . Please note that only the points exactly on this circle represent  $V_i(s) = X$ , the points inside or outside this circle do not mean  $V_i(s) < X$  nor  $V_i(s) > X$ . For better illustration, Fig. 5 is used to show the formation process of voltage safety region. In Fig. 5, we assume that the voltage value of  $V_i(s)$  ranges within [0.90 p.u., 1.10 p.u.]. Each voltage value can form a circle on the  $\sigma$  complex plane, e.g., six circles in Fig. 5 formed respectively by  $V_i(s) = 0.90$  p.u., 0.93 p.u., 0.98 p.u., 1.02 p.u., 1.06 p.u., and 1.10 p.u. The points on these 6 circles represent the corresponding voltage values. In a similar way, an infinite number of voltage values within [0.90 p.u., 1.10 p.u.] can form an infinite number of circles on the  $\sigma$  complex plane. All points on all circles can form a region, i.e., the red

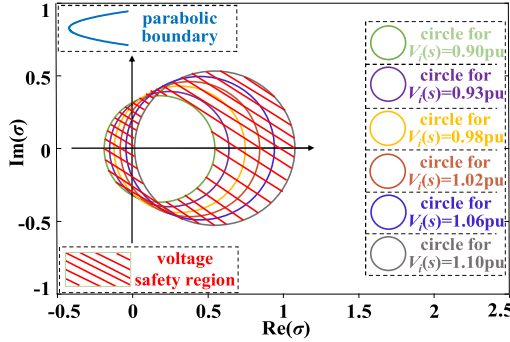


Fig. 5. The formation process of visualized voltage safety region.

striped region in Fig. 5, which is the visualized voltage safety region representing the voltage range [0.90 p.u., 1.10 p.u.]. It can be found in Fig. 5, the largest circle (i.e., the upper limit 1.10 p.u.) and the smallest circle (i.e., the lower limit 0.90 p.u.) are both on the outer boundary of the voltage safety region. This is reasonable because the voltage violations can be triggered by both the upper violation (i.e., voltage index  $\sigma_i(s)$  exits from the safety region by crossing the largest circle part) and the lower violation (i.e., voltage index  $\sigma_i(s)$  exits from the safety region by crossing the smallest circle part), which depends on the actual operating conditions.

### B. Visualization of Bus-Specific Var Safety Region

Since the Var violations of generators may deteriorate the voltage security, it is necessary to monitor these undesired events. Rewrite (1) with holomorphic embedding,

$$\sigma_i(s) = \frac{Z_i(s)S_i^*(s^*)}{|V_{sw}|^2}, \forall i \in \mathcal{P} \quad (8)$$

where  $S_i^*(s^*) = sP_i - jQ_i(s)$  is for generator bus  $i$ ,  $Z_i(s) = R_i(s) + jX_i(s)$  is the virtual line impedance on channel  $i$ . Then, separate (8) into real and imaginary parts, and eliminate  $|V_{sw}|^2$ ,

$$\sigma_{iI}(s) = \frac{X_i(s) \cdot s \cdot P_i - R_i(s)Q_i(s)}{X_i(s)Q_i(s) + R_i(s) \cdot s \cdot P_i} \cdot \sigma_{iR}(s), \forall i \in \mathcal{P} \quad (9)$$

It can be found in (9), the real and imaginary parts of generator Var index  $\sigma_i(s)$  form a straight line on the  $\sigma$  complex plane, and the slope of the straight line depends on the  $s$  value.

1) For the transmission networks: In general, compared with the reactance, the resistance can be assumed to be 0 in the transmission network (i.e.,  $X \gg R$ ) [3]. (The implications of excluding the resistance parameter will be analyzed in Section V-B). Thus, (9) can be simplified to (10) by setting  $R_i(s)$  to 0 and eliminating  $X_i(s)$ .

$$\sigma_{iI}(s) \approx \frac{s \cdot P_i}{Q_i(s)} \cdot \sigma_{iR}(s), \forall i \in \mathcal{P} \quad (10)$$

Based on (10), operators can preset the Var range flexibly according to different operating requirements, e.g., the Var at generator bus  $i$  is set to  $Q_{iL} \leq Q_i \leq Q_{iH}$ . Then, by substituting  $Q_{iL}$  and  $Q_{iH}$  into (10), the Var limits  $Q_{iL}$  and  $Q_{iH}$  can be projected onto the  $\sigma$  complex plane as two straight lines, which go through the origin point with gradients of  $sP_i/Q_{iL}$  and  $sP_i/Q_{iH}$ , respectively, as shown in Fig. 6. The voltage collapse boundary is represented by the blue parabola, the lower and upper Var limits are visualized as the orange and red straight lines, respectively. Thus, the grey part, which is surrounded by the above three boundaries, denotes the Var safety region. By plotting the trajectory of index  $\sigma_i(s)$  on Fig. 6, operators can visually monitor the Var status of generators and predict the Var violations (demonstrated in Section V-B).

2) For the distribution networks: The resistance parameter in (9) cannot be neglected since it will obviously affect the Var safety region for distribution networks. Thus, operators should follow (9) strictly to visualize the Var safety region.

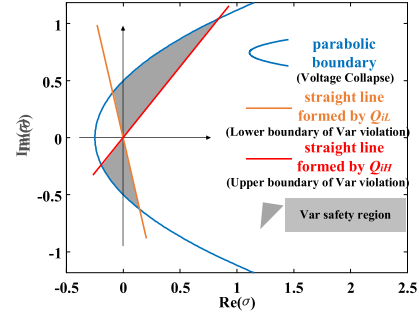


Fig. 6. Visualization of Var safety region and boundaries.

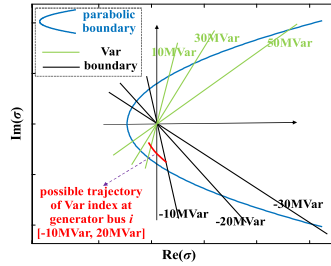


Fig. 7. Illustration of multiple preset Var boundaries and a possible trajectory of generator Var index.

*Remark:* The formation process of Var safety region is similar to that of the Volt safety region illustrated in Fig. 5.

### C. Discussions on Boundary Range and Operating Range

For the scenarios that the critical boundary range is much larger than the range of the changes in operating point, operators can artificially preset multiple desired Volt/Var boundary ranges, which can be defined flexibly to make the preset Volt/Var boundary ranges close to the operating range. Thus, the visualization results can be more convenient for operators to visually monitor the Volt/Var status and predict their violations. For example, in Fig. 7, we assume the critical boundary range of generator Var  $Q_i$  is  $-30\text{MVar} < Q_i < 50\text{MVar}$ , and its operating point may only range within  $[-10\text{MVar}, 20\text{MVar}]$ , which is much smaller than its critical boundary range. In this scenario, operators can artificially preset multiple desired Var boundary ranges (i.e., multiple straight lines in Fig. 7), e.g.,  $[-10\text{MVar}, 10\text{MVar}]$ ,  $[-20\text{MVar}, 30\text{MVar}]$ , and  $[-30\text{MVar}, 50\text{MVar}]$ . These preset Var boundary ranges are close to the operating range. Thus, the operators can visually monitor the generator Var status and predict if the generator will violate the desired Var boundary ranges.

## V. CASE STUDY AND RESULTS ANALYSIS

The case study is conducted on the IEEE 14-bus transmission system. The trajectory of Volt/Var index is derived in MATPOWER 4.1 [9] with power flow tolerance of  $10^{-6}$  p.u.

### A. Illustration of Bus-Specific Voltage Safety Region

For the sake of illustration, a unified voltage range is introduced for all buses, i.e.,  $V_L = 0.90$  p.u. and  $V_H = 1.10$  p.u., and the system load increases from the base, i.e.,  $s = 1.00$  p.u. As shown in Fig. 8, the trajectory of the index at bus 14 first intersects the circle boundary formed by  $V_L = 0.90$  p.u. with  $s = 1.60$  p.u., which means the voltage of bus 14 will violate the lower limit ( $V_L = 0.90$  p.u.) if the system load increases to 1.60 times of the base. Thus, using the proposed Volt safety region, operators can visually monitor the voltage status of each bus and foresee which bus voltage will violate the limits.

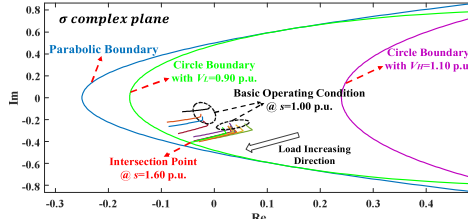


Fig. 8. Illustration of the trajectories of indices, voltage safety region and boundaries when system load increases from  $s = 1.00$  p.u. to  $s = 1.60$  p.u.

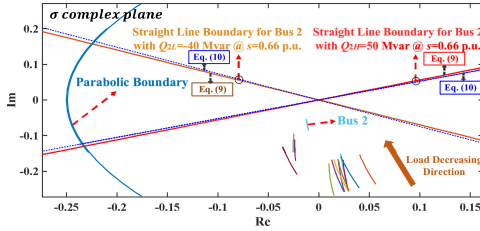


Fig. 9. Illustration of the trajectories of indices, Var safety region and boundaries when system load decreases from  $s = 1.00$  p.u. to  $s = 0.66$  p.u.

### B. Illustration of Bus-Specific Var Safety Region

Here, we assume the Var at generator bus 2 is constrained by a lower limit  $Q_{2L} = -40$  MVar and an upper limit  $Q_{2H} = 50$  MVar. As demonstrated in Fig. 9, by using (9) and (10), the visualized straight lines representing the Var safety boundaries are nearly the same, which means the exclusion of the resistance parameter in (9) will not result in considerable under/over-estimation of the Var safety margin. When the system load decreases from the base ( $s = 1.00$  p.u.) to  $s = 0.66$  p.u., the trajectory of the index at generator bus 2 is approaching to its boundary but does not touch it, which means the generator at bus 2 will not violate its Var limits if the system load reduces to 0.66 times of the base. This judgment is credible since any Var violation will result in the discontinuity of the trajectories. However, all trajectories shown in Fig. 9 are continuous. Thus, by using the proposed Var safety region, operators can visually monitor the Var status of generators and judge if any generator violates its Var limits.

## VI. CONCLUSION

This letter proposes a visualized method to monitor the Volt/Var status of each bus and predict the violations. Firstly, based on nonlinear network decomposition, an index representing the Volt/Var status is introduced. Then, a scalable holomorphic embedding method is adopted to obtain the trajectory of Volt/Var index under prospective operating conditions. Finally, bus-specific Volt/Var safety regions are visualized to foresee the violations. Test results on the IEEE 14-bus system show the great potential of the proposed method in Volt/Var monitoring and violation predicting.

## APPENDIX

### A. Solving Procedure of $\sigma(s)$

$\sigma(s)$  is solved by combining (4) and the holomorphic embedded power flow equations (HEPFE). Different forms of HEPFE can be adopted for different scenarios [4], [6], [7]. In this letter, (A1) in [4] is taken for an illustration, where the loads are increased by  $ss_i^*$ , the reactive power of each generator is re-dispatched by  $Q_i(s)$  to keep the voltage magnitude of PV bus invariant, and the active power of each generator is re-dispatched

by  $sP_i$ .

$$\begin{cases} \sum_{k=1}^N Y_{ik} V_k(s) = \frac{sS_i^*}{V_i^*(s^*)}, & \forall i \in \mathcal{M} \\ \sum_{k=1}^N Y_{ik} V_k(s) = \frac{sP_i - jQ_i(s)}{V_i^*(s^*)} \text{ and } V_i(s)V_i^*(s^*) \\ = |V_i^{sp}|^2, & \forall i \in \mathcal{P} \end{cases} \quad (\text{A1})$$

where  $Y_{ik}$  is the  $(i,k)$  element of admittance matrix including the branch susceptance, transformer taps, capacitor banks *et al.*. In general, there are  $(4m+5p)$  real-valued *unknowns* and  $(4m+5p)$  real-valued equations in (4) and (A1), which means solvable. The detailed procedure can be found in Eq. (11)–(20) of [4]. Besides, other forms of HEPFE [6], [7] can also be easily combined with the proposed method in a similar way.

### B. Update $\sigma(s)$ When Network Topology Changes

When the network topology changes, the original admittance matrix  $Y_{ik}$  in (A1) should be modified to  $Y_{ik-m}$  according to the topology change. Then,  $\sigma(s)$  for the changed network topology need to be updated and resolved by combining (4) and the new HEPFE with modified admittance matrix  $Y_{ik-m}$ .

### C. Mathematical Complexity and Computational Effort

To recalculate the  $\sigma(s)$ , one can combine (4) and the new HEPFE with modified admittance matrix  $Y_{ik-m}$ , and equate the coefficients of  $s$  with the same order at both sides to construct a recursive relation (A2) between the current *unknown* term [B] and its previous *known* terms [C].

$$[\mathbf{A}]_{(4m+5p) \times (4m+5p)} \cdot [\mathbf{B}]_{(4m+5p) \times 1} = [\mathbf{C}]_{(4m+5p) \times 1} \quad (\text{A2})$$

where [A] is a constant matrix in the recursion process, and [C] contains a number of  $(2m+5p)$  discrete convolution. Thus, according to the arithmetic analysis of computational complexity [8], the overall mathematical complexity up to the  $H^{\text{th}}$  order is  $O((2m+5p) \cdot H \cdot \log H)$ . For example, the computational effort for  $\sigma(s)$  in Case B is about 1.63s.

## REFERENCES

- [1] H. Chiang, A. J. Flueck, K. S. Shah, and N. Balu, "CPFLOW: A practical tool for tracing power system steady-state stationary behavior due to load and generation variations," *IEEE Trans. Power Syst.*, vol. 10, no. 2, pp. 623–634, May 1995.
- [2] Q. Lai, C. Liu, and K. Sun, "Analytical static voltage stability boundary based on holomorphic embedding," *Int. J. Elect. Power Energy Syst.*, vol. 134, Jan. 2022, Art. no. 107386.
- [3] P. Kundur, *Power System Stability and Control*. New York, NY, USA: McGraw-Hill, 1994.
- [4] Q. Lai, C. Liu, and K. Sun, "Vulnerability assessment for voltage stability based on solvability regions of decoupled power flow equations," *Appl. Energy*, vol. 304, Dec. 2021, Art. no. 117738.
- [5] A. Trias, "Sigma algebraic approximants as a diagnostic tool in power networks," U.S. Patent 2014/0156094, 2014.
- [6] C. Liu, B. Wang, F. Hu, K. Sun, and C. L. Bak, "Online voltage stability assessment for load areas based on the holomorphic embedding method," *IEEE Trans Power Syst.*, vol. 33, no. 4, pp. 3720–3734, Jul. 2018.
- [7] C. Liu, B. Wang, X. Xu, K. Sun, D. Shi, and C. L. Bak, "A multi-dimensional holomorphic embedding method to solve AC power flows," *IEEE Access*, vol. 5, no. 1, pp. 25270–25285, Dec. 2017.
- [8] S. Arora and B. Barak, *Computational Complexity: A Modern Approach*. Cambridge, U.K.: Cambridge Univ. Press, 2009.
- [9] R. D. Zimmerman, C. E. Murillo-Sánchez, and R. J. Thomas, "MATPOWER: Steady-state operations, planning, and analysis tools for power systems research and education," *IEEE Trans. Power Syst.*, vol. 26, no. 1, pp. 12–19, Feb. 2011.